Research Square

Preprints are preliminary reports that have not undergone peer review.
They should not be considered conclusive, used to inform clinical practice,
or referenced by the media as validated information.

Dopaminergic signalling through dopamine receptor D2 favours the functional stability of regulatory T cells mitigating gut inflammation and neuroinflammation

Jazmín Castro
San Sebastián University
José Manuel Jiménez
Fundación Ciencia and Vida
Daniela Elgueta
Fundación Ciencia and Vida
Ornella Chovar
Fundación Ciencia and Vida
Valentina Ugalde-Tagle
Fundación Ciencia and Vida
Nicolás Martínez
Fundación Ciencia and Vida
Javiera Cea
San Sebastián University
Alexandra Espinoza
Fundación Ciencia and Vida
Jacob Mora
Fundación Ciencia and Vida
Sebastián Valenzuela
Fundación Ciencia and Vida
Micaela Ricca
Fundación Ciencia and Vida
Carolina Prado
San Sebastián University
Rodrigo Pacheco
rpacheco@cienciavida.org

Fundación Ciencia and Vida

Research Article

Keywords:

Posted Date: October 30th, 2026

DOI: https://doi.org/10.21203/rs.3.rs-10670304/v1

License: This work is licensed under a Creative Commons Attribution 4.0 International License.
Read Full License

Additional Declarations: No competing interests reported.

Abstract

Parkinson's disease (PD) is characterised by progressive dopaminergic neurodegeneration, α-synuclein (αSyn) accumulation and chronic neuroinflammation. Regulatory T (Treg) cells restrain inflammatory responses in both the central nervous system and the intestine, but the mechanisms controlling their function during PD remain incompletely understood. Here, we investigated the role of dopamine receptor D2 (Drd2) signalling in T-cells, with particular emphasis on Treg differentiation, phenotypic stability and suppressive activity. Using an AAV-αSyn model of PD, we found that *Drd2* deficiency in $CD4^+$ T-cells exacerbated neuroinflammation, dopaminergic neuronal loss and motor impairment, whereas selective *Drd2* deficiency in $CD8^+$ T-cells did not reproduce this phenotype. *Drd2* deficiency in $CD4^+$ T-cells selectively increased T-cell infiltration into the SN, while reducing the frequency of splenic Treg cells without affecting Th1, Th17 or TNF-α-producing $CD4^+$ T-cell subsets. In vitro, *Drd2*-deficient naïve $CD4^+$ T-cells displayed impaired differentiation into $Foxp3^+$ Treg cells and reduced TGF-β production. Moreover, activated *Drd2*-deficient Treg cells exhibited decreased Foxp3 expression and increased production of IL-17 and IFN-γ without altered viability. In a model of dextran sodium sulphate-induced colitis, adoptively transferred *Drd2*-deficient Treg cells failed to attenuate body-weight loss and colon shortening. Although their recruitment to the colonic lamina propria was preserved, these cells showed reduced maintenance of Foxp3 expression. Collectively, these findings identify Drd2 signalling as a key regulator of Treg differentiation, phenotypic stability and suppressive function, thereby limiting intestinal inflammation and αSyn-associated dopaminergic neurodegeneration.

Introduction

Parkinson's disease (PD) is the second most common neurodegenerative disorder and is characterised by the progressive loss of dopaminergic neurons in the nigrostriatal pathway, leading to motor manifestations including bradykinesia, rigidity, resting tremor, and postural instability. Neuropathologically, PD is also defined by the accumulation of misfolded α-synuclein (αSyn) aggregates that form Lewy bodies and Lewy neurites throughout the central and peripheral nervous systems (Braak et al., 2003; Lim and Zhang, 2013). Although αSyn aggregation and dopaminergic neurodegeneration are central hallmarks of the disease, increasing evidence indicates that chronic neuroinflammation is a major driver of disease progression (Gonzalez and Pacheco, 2014). Pathogenic forms of αSyn activate innate immune responses through pattern-recognition receptors, promoting microglial activation and the production of neurotoxic mediators that contribute to neuronal damage (Kim et al., 2013; Noelker et al., 2013; Gonzalez and Pacheco, 2014).

Beyond innate immunity, adaptive immune responses have emerged as critical regulators of PD pathogenesis. Both experimental models and studies in patients have demonstrated the presence of αSyn-specific T-cell responses, as well as infiltration of $CD4^+$ and $CD8^+$ T cells into affected brain regions (Roodveldt et al., 2024). Importantly, distinct $CD4^+$ T-cell subsets exert opposing effects on neuroinflammation. Whereas Th1 and Th17 cells promote pro-inflammatory microglial activation and neurodegeneration, regulatory T cells (Treg) suppress inflammatory responses and favour

neuroprotective mechanisms (Gonzalez et al., 2015). Accordingly, modulation of T-cell function has become an attractive therapeutic strategy for limiting disease progression in PD (Pacheco, 2021).

Recent findings have further strengthened the concept that PD is not solely a brain disorder but may originate in the gastrointestinal tract. According to the Braak hypothesis, pathological αSyn accumulation may begin in the enteric nervous system and subsequently spread to the brain through anatomically connected pathways (Braak et al., 2003). Consistent with this view, intestinal inflammation, alterations in gut barrier integrity, and immune dysregulation are increasingly recognised as early events in PD pathogenesis (Campos-Acuna et al., 2019). Epidemiological and experimental evidence has also revealed a close association between inflammatory bowel diseases (IBD) and PD, suggesting that common immune mechanisms may contribute to both conditions. In the intestine, immune homeostasis depends on a tightly regulated balance between inflammatory effector T-cells and Treg cells. While Th1 and Th17 responses drive intestinal inflammation, Treg-derived interleukin-10 (IL-10) and transforming growth factor-β (TGF-β) are essential for maintaining mucosal tolerance and preventing excessive immune activation (Huber et al., 2004; Rubtsov et al., 2008; Wu et al., 2014).

Dopamine represents an important molecular link between the nervous and immune systems. In addition to its well-established role as a neurotransmitter, dopamine regulates the activity, differentiation, and migration of immune cells through five G-protein-coupled receptors, designated DRD1–DRD5 (Alexander et al., 2023). These receptors display markedly different affinities for dopamine, allowing immune cells to sense and respond to changes in local dopamine concentrations (Pacheco et al., 2014). In inflammatory environments, where dopamine levels are substantially reduced, signalling through high-affinity receptors is favoured. In this regard, our previous studies demonstrated that DRD3 signalling in $CD4^+$ T-cells favours Th1 and Th17 responses while limiting the suppressive function of Treg cells, thereby exacerbating intestinal inflammation and promoting neurodegeneration in experimental models of PD (Gonzalez et al., 2013; Franz et al., 2015; Contreras et al., 2016; Elgueta et al., 2017; Elgueta et al., 2019; Ugalde et al., 2021). By contrast, accumulating evidence suggests that DRD2 signalling exerts predominantly anti-inflammatory effects. Activation of DRD2 promotes IL-10 production by human $CD4^+$ T cells, attenuates inflammatory responses in several disease models, and contributes to tissue protection in both peripheral and central inflammatory conditions (Besser et al., 2005; Shao et al., 2013; Liu et al., 2021; Mora et al., 2025).

Interestingly, evidence from the 1-methyl-4-phenyl-1,2,3,6-tetrahydropyridine (MPTP)-induced mouse model of Parkinson's disease indicates that DRD2 signalling in $CD4^+$ T cells exerts a protective effect against neuroinflammation and dopaminergic neurodegeneration (Liu et al., 2021). Moreover, in a previous study, we demonstrated that DRD2 signalling in T cells attenuated intestinal inflammation *in vivo*, an effect associated with enhanced suppressive activity of regulatory T cells (Treg) *in vitro* (Mora et al., 2025). However, the functional significance of DRD2 signalling in Treg cells *in vivo* has yet to be determined.

Given the emerging relevance of adaptive immunity in PD and the growing recognition of the gut–brain axis in disease initiation, understanding how dopaminergic signalling regulates T-cell function has become a key question. In particular, whether DRD2 signalling controls Treg-mediated immunoregulation in both intestinal inflammation and PD-associated neuroinflammation remains unknown. In the present study, we investigated the role of DRD2 expressed by T cells, with a special focus on Treg function, using conditional Drd2-deficient mice. Considering that intestinal inflammation is increasingly viewed as a relevant component of PD pathogenesis, we examined the contribution of DRD2 signalling to immune regulation in the gut and evaluated how this pathway influences T-cell responses associated with neurodegenerative disease. Our findings identify DRD2 as an important regulator of Treg-mediated immune homeostasis and provide new insights into dopaminergic mechanisms controlling intestinal inflammation and neuroinflammation.

Results

Drd2 deficiency in CD4$^+$ T-cells increases dopaminergic neurodegeneration and motor decline in AAV-αSyn-treated mice

A previous study showed that *CD4^{Cre}Drd2$^{f/f}$* mice exhibit exacerbated dopaminergic neuronal loss and motor impairment following MPTP treatment (Liu et al., 2021). However, during the thymic development of αβ T-cells in *CD4^{Cre}* mice, floxed genes are deleted at the double-positive CD4$^+$CD8$^+$ thymocyte stage, resulting in their deletion in both mature CD4$^+$ and CD8$^+$ T-cells (Lee et al., 2001). To determine the specific contribution of Drd2 signalling in CD4$^+$ and CD8$^+$ T-cells to dopaminergic neurodegeneration, we compared dopaminergic neuronal loss in *CD4^{Cre}Drd2$^{f/f}$* mice, in which *Drd2* is deficient in both CD4$^+$ and CD8$^+$ T-cells, with that observed in *CD8^{Cre}Drd2$^{f/f}$* mice, in which *Drd2* deficiency is restricted to CD8$^+$ T cells (Maekawa et al., 2008). For this purpose, we used a preclinical model of PD in which neurodegeneration is induced by unilateral stereotaxic delivery of adeno-associated viral vectors encoding *SNCA* (AAV-αSyn) into the substantia nigra (SN), as this model involves an antigen-specific T-cell response against αSyn-derived antigens (Roodveldt et al., 2024). As we anticipated that *Drd2* deficiency in T-cells would exacerbate AAV-αSyn-induced neurodegeneration, we used a suboptimal dose of AAV-αSyn. Interestingly, *CD4^{Cre}Drd2$^{f/f}$* mice, but not *CD8^{Cre}Drd2$^{f/f}$* mice, showed a significant reduction in dopaminergic neuronal density on the ipsilateral side relative to the contralateral side (**Fig. 1A–B**). Consistent with this finding, significant motor impairment was observed only in *CD4^{Cre}Drd2$^{f/f}$* mice and not in *CD8^{Cre}Drd2$^{f/f}$* mice (**Fig. 1C**). Collectively, these results indicate that Drd2 signalling in CD4$^+$ T cells, but not in CD8$^+$ T cells, exerts a protective effect by limiting the extent of AAV-αSyn-induced neurodegeneration and the consequent motor impairment.

Drd2 deficiency in CD4$^+$ T-cells enhances neuroinflammation in AAV-αSyn-treated mice

Neuroinflammation is a critical process that contributes to neurodegeneration in PD, and T-cells are key players in promoting neuroinflammation by exacerbating microglial responses in the brain (Roodveldt et

al., 2024). To investigate the relevance of *Drd2* signalling in $CD4^+$ T-cells to the development of neuroinflammation, we next analysed the extent of T-cell infiltration into the brain. Our results showed that *Drd2* deficiency in $CD4^+$ T-cells increased $CD4^+$ T-cell infiltration into the SN without affecting $CD8^+$ T-cell infiltration in AAV-αSyn-treated mice (**Fig. 2A–B**). Conversely, *Drd2* deficiency in $CD8^+$ T cells affected the infiltration of neither $CD4^+$ nor $CD8^+$ T-cells into the SN (**Fig. 2A–B**).

We next asked whether the increased $CD4^+$ T-cell infiltration induced by *Drd2* deficiency was associated with altered microglial reactivity. To address this, we analysed microglial TREM2 expression. Increased TREM2 expression is consistent with a shift towards a phagocytic, damage-responsive microglial phenotype (Deczkowska et al., 2018). Although *Drd2* deficiency in $CD4^+$ T-cells did not affect overall Iba1 immunoreactivity, it increased TREM2 expression in the SN of AAV-αSyn-treated mice (**Fig. 3A–B**). Consistent with the absence of increased $CD4^+$ T-cell infiltration, *Drd2* deficiency in $CD8^+$ T-cells did not affect either TREM2 expression or Iba1 immunoreactivity in the SN of AAV-αSyn-treated mice (**Fig. 3A–B**). Together, these results suggest that Drd2 signalling in $CD4^+$ T-cells limits their infiltration into the SN and the associated induction of a TREM2-positive, damage-responsive microglial phenotype in this mouse model.

Drd2 deficiency in T-cells is associated with limited Tregs generation and phenotypic stability in vitro

As selective *Drd2* deficiency in $CD4^+$ T-cells exacerbated neuroinflammation, neurodegeneration and motor impairment in AAV-αSyn-treated mice, we sought to elucidate the underlying mechanism. To this end, we investigated how Drd2 signalling affected distinct $CD4^+$ T-cell subsets in AAV-αSyn-treated mice. Once neuroinflammation, neurodegeneration and motor impairment had developed, the frequencies of functional $CD4^+$ T-cell subsets in the spleen were analysed by flow cytometry. The results showed that *Drd2* deficiency in $CD4^+$ T-cells selectively reduced the frequency of regulatory T (Treg) cells without affecting the frequencies of pro-inflammatory subsets, including Th1, Th17, and TNF-α-producing $CD4^+$ T cells (**Fig. 4A–B**).

To determine whether the reduced frequency of Treg cells observed in $CD4^{Cre}Drd2^{f/f}$ mice resulted from impaired Treg differentiation, reduced phenotypic stability, or increased cell death, we performed *in vitro* differentiation and transdifferentiation assays. Treg differentiation was induced in naïve $CD4^+$ T-cells isolated from WT or $CD4^{Cre}Drd2^{f/f}$ $Foxp3^{GFP}$ reporter mice, and phenotypic and functional parameters were assessed five days later. *Drd2* deficiency selectively reduced the frequency of $Foxp3^+$ (GFP^+) Treg cells and impaired TGF-β production without affecting IL-10 production (**Fig. 5A**).

To complement these findings, we performed *in vitro* transdifferentiation assays in which Treg cells isolated from WT $Foxp3^{GFP}$ or $CD4^{Cre}Drd2^{f/f}$ $Foxp3^{GFP}$ reporter mice were activated in the absence or presence of 2 μM dopamine, a concentration capable of activating Drd2 (Sokoloff et al., 1990). After 72 h of stimulation, the functional phenotype of the T-cells was assessed by analysing the expression of Foxp3, IL-17, and IFN-γ. In the presence of dopamine, *Drd2*-deficient Treg cells exhibited reduced Foxp3

expression and increased production of the pro-inflammatory cytokines IL-17 and IFN-γ (**Fig. 5B**). Notably, Drd2 deficiency did not affect Treg-cell viability (**Fig. 5B**). Collectively, these results indicate that Drd2 signalling promotes Treg differentiation and phenotypic stability *in vitro* without affecting cell viability.

Drd2 deficiency in CD4$^+$ T-cells limits phenotypic Treg stability in vivo

The findings described above suggest that the reduced Treg frequency observed in *Drd2*-deficient mice may result from impaired Treg generation and stability under inflammatory conditions. To investigate whether *Drd2* deficiency compromises Treg phenotypic stability, and given that the neuroinflammation associated with Parkinson's disease has been linked to preceding intestinal inflammation, we next performed experiments in which WT or *Drd2*-deficient Treg cells were transferred into mice undergoing gut inflammation. Their suppressive activity and phenotypic stability were subsequently assessed *in vivo*.

For this purpose, we used a model of intestinal inflammation induced by the administration of dextran sodium sulphate (DSS) in the drinking water. DSS disrupts the integrity of the intestinal epithelial barrier, triggering acute inflammation that leads to colitis and body-weight loss (Huber et al., 2004). To determine how Drd2 signalling affected the suppressive capacity of Treg cells, we transferred WT or *Drd2*-deficient Treg cells into DSS-treated mice and monitored disease manifestations over the following seven days. WT Treg cells substantially attenuated disease severity. By contrast, *Drd2*-deficient Treg cells failed to reduce either body-weight loss (**Fig. 6A**) or colon shortening (**Fig. 6B**).

To assess the effect of *Drd2* deficiency on Treg stability, the frequency of Foxp3$^+$ cells was determined seven days after Treg transfer among donor cells that had migrated to the colonic lamina propria (cLP). Interestingly, *Drd2* deficiency did not affect the recruitment of donor Treg cells to the cLP (**Fig. 6C**), but resulted in a marked reduction in Foxp3 expression among donor cells reaching this compartment (**Fig. 6D**). Collectively, these results indicate that Drd2 signalling supports Treg phenotypic stability, thereby promoting their suppressive activity *in vivo*.

Discussion

The present study identifies Drd2 signalling in CD4$^+$ T-cells as an immunoregulatory pathway that limits αSyn-associated dopaminergic neurodegeneration and motor dysfunction. *Drd2* deficiency in the T-cell compartment exacerbated dopaminergic neuronal loss and motor impairment following nigral delivery of AAV-αSyn, whereas selective *Drd2* deficiency in CD8$^+$ T-cells did not reproduce this phenotype. Mechanistically, the detrimental consequences of *Drd2* deficiency were associated with a selective reduction in the frequency of Treg cells, impaired differentiation of naïve CD4$^+$ T-cells into Foxp3$^+$ Treg cells, and reduced Treg phenotypic stability under inflammatory conditions. Furthermore, adoptively transferred *Drd2*-deficient Treg cells failed to control DSS-induced intestinal inflammation despite reaching the colonic lamina propria normally, and this impaired suppressive activity was accompanied

by reduced maintenance of Foxp3 expression. Collectively, these findings indicate that Drd2 signalling contributes to immune homeostasis by supporting both the generation and functional stability of Treg cells.

An important feature of the present work is the use of an αSyn-driven model of Parkinson's disease. Previous evidence demonstrating a protective effect of Drd2 expressed by CD4⁺ T-cells was obtained using the MPTP model, in which neuronal damage is initiated by an acute neurotoxic insult (Liu et al., 2021). By contrast, the AAV-αSyn model involves sustained expression of a disease-relevant protein and incorporates adaptive immune responses directed against αSyn-derived antigens. This distinction is particularly relevant because αSyn-reactive CD4⁺ and CD8⁺ T-cells have been identified in patients with Parkinson's disease, and their responses appear to be most prominent during prodromal and early clinical stages of the disease (Sulzer et al., 2017; Lindestam Arlehamn et al., 2020). Our results therefore extend the protective role of T-cell Drd2 beyond toxin-induced neurodegeneration and show that this pathway also restrains neuronal damage in a model involving a clinically relevant autoantigen.

The absence of an overt phenotype in AAV-αSyn-treated *CD8^{Cre}Drd2$^{f/f}$* mice suggests that the enhanced neurodegeneration observed in *CD4^{Cre}Drd2$^{f/f}$* mice is primarily attributable to the loss of Drd2 signalling within the CD4⁺ T-cell compartment. This finding does not imply that CD8⁺ T-cells are dispensable in Parkinson's disease, as cytotoxic T-cell infiltration has been detected in the substantia nigra and may precede overt αSyn pathology and neuronal loss (Galiano-Landeira et al., 2020). Rather, the present data indicate that Drd2 expressed by CD8⁺ T-cells is not a major determinant of the neuroprotective effect identified under our experimental conditions. Because *CD4^{Cre}*-mediated recombination occurs at the CD4⁺CD8⁺ thymocyte stage and consequently affects both mature CD4⁺ and CD8⁺ T-cells, comparison with *CD8^{Cre}Drd2$^{f/f}$* mice provides an important means of narrowing the relevant phenotype to CD4⁺ T-cells. Nevertheless, experiments using a Treg-specific conditional knockout will ultimately be required to establish whether the neuronal phenotype is caused directly by the absence of *Drd2* in Treg cells.

Our findings are consistent with a broader anti-inflammatory role for Drd2 in immune regulation. Dopamine acting through D2-like receptors induces IL-10 production by human T-cells, while activation of lymphocyte Drd2 improves the Th17/Treg balance and attenuates inflammatory disease in experimental arthritis (Besser et al., 2005; Lu et al., 2015). These effects contrast with those attributed to Drd3, which promotes Th1 and Th17 differentiation and contributes to T-cell-mediated neuroinflammation (Gonzalez et al., 2013; Elgueta et al., 2019). Dopaminergic signalling through Drd3 has also been shown to limit Treg suppressive activity and intestinal homing during gut inflammation (Ugalde et al., 2021). More recently, the DRD2:DRD3 heteromer was identified as a dopamine-sensing complex that regulates both the recruitment and suppressive activity of intestinal Treg cells (Mora et al., 2025). Together, these observations indicate that dopamine does not exert a uniformly pro- or anti-inflammatory effect on T-cells. Instead, its immunological consequences depend on the receptor subtype, receptor organisation, cellular differentiation state and inflammatory context.

A central observation of the present study was that Drd2 deficiency selectively reduced the frequency of Treg cells without detectably altering the frequencies of Th1, Th17 or TNF-α-producing $CD4^+$ T-cells in the spleen. This pattern argues against a generalised effect of Drd2 on $CD4^+$ T-cell activation and instead suggests a preferential requirement for Drd2 in maintaining the regulatory compartment. Treg cells have previously been shown to protect the nigrostriatal system by suppressing inflammatory microglial responses and promoting a neuroprotective tissue environment. Indeed, adoptive transfer of activated Treg cells markedly reduces MPTP-induced dopaminergic neurodegeneration, whereas effector T-cells do not confer comparable protection (Reynolds et al., 2007). Thus, even in the absence of a measurable systemic increase in conventional pro-inflammatory $CD4^+$ T-cell subsets, a selective reduction in Treg abundance or function may shift the balance of the immune response sufficiently to enhance αSyn-associated neuronal damage.

In addition to impaired differentiation, our findings indicate that Drd2 contributes to the maintenance of the Treg phenotype after activation. In the presence of dopamine, *Drd2*-deficient Treg cells displayed reduced Foxp3 expression and increased production of IL-17 and IFN-γ without a corresponding reduction in viability. These results favour phenotypic destabilisation rather than preferential death of *Drd2*-deficient Treg cells. Stable Foxp3 expression is required to preserve the transcriptional and functional identity of Treg cells, whereas inflammatory environments can induce loss of regulatory features and derepression of conventional effector T-cell programmes (Chen et al., 2013; Garg et al., 2019; Helmin et al., 2020). The acquisition of IL-17 and IFN-γ production may be particularly relevant to neurodegenerative disease because it could generate a dual pathogenic effect: loss of suppressive activity together with acquisition of pro-inflammatory functions capable of amplifying tissue inflammation. Nevertheless, the present experiments demonstrate loss of the contemporary $Foxp3^+$ phenotype rather than definitive lineage conversion. An irreversible Foxp3 fate-mapping system would be required to establish whether these cells become bona fide ex-Treg cells and persist as pathogenic effector populations.

The adoptive-transfer experiments provide strong evidence that Drd2 has a Treg-intrinsic role during intestinal inflammation. WT Treg cells attenuated body-weight loss and colon shortening in DSS-treated recipients, whereas *Drd2*-deficient Treg cells failed to confer comparable protection. Importantly, *Drd2* deficiency did not reduce the abundance of donor cells reaching the colonic lamina propria, but markedly decreased the proportion of donor cells retaining Foxp3 expression. These findings distinguish tissue recruitment from phenotypic maintenance and indicate that Drd2 is required principally for the preservation of Treg identity and suppressive activity after entry into an inflamed tissue. The apparently preserved migration observed here differs from our previous findings (Mora et al., 2025). This discrepancy may reflect differences in the timing of analysis of donor Treg cells after their migration to the colonic lamina propria (cLP): two days after transfer in our previous study and seven days after transfer in the present study. These different time points suggest that *Drd2*-deficient Treg cells may migrate more slowly than WT Treg cells into the cLP. By day 7, when the recruitment of WT and Drd2-deficient donor cells was comparable, a significantly greater proportion of *Drd2*-deficient cells had lost the Treg phenotype and acquired pro-inflammatory features.

The present study does not directly demonstrate that instability of intestinal Treg cells causes the enhanced nigral neurodegeneration observed in *CD4^{Cre}Drd2$^{f/f}$* mice. The DSS and AAV-αSyn experiments were performed as complementary models addressing the intestinal and neurological consequences of *Drd2* deficiency, respectively. Establishing a causal gut–immune–brain sequence will require experiments combining intestinal inflammation with αSyn-driven neurodegeneration. It would be particularly informative to determine whether intestinal inflammation exacerbates the neuronal phenotype of *CD4^{Cre}Drd2$^{f/f}$* mice, whether adoptive transfer of WT Treg cells rescues this effect, and whether donor Treg cells or their descendants can be tracked from intestinal lymphoid tissues to systemic or brain-associated immune compartments.

The intracellular mechanism through which Drd2 maintains Foxp3 expression remains to be established. Drd2 can activate both canonical Gi/o-dependent pathways and β-arrestin-dependent signalling. In astrocytes, Drd2 suppresses inflammatory responses through αB-crystallin and inhibits NLRP3 inflammasome activation through a β-arrestin-2-dependent mechanism (Shao et al., 2013; Zhu et al., 2018). Although these findings cannot be directly extrapolated to Treg cells, they demonstrate that Drd2 engages cell-specific anti-inflammatory signalling modules. Future studies should determine whether Drd2 regulates the IL-2–STAT5, TGF-β–SMAD, PI3K–AKT–mTOR or β-arrestin pathways in Treg cells. It will also be important to assess whether Drd2 influences the epigenetic programme that stabilises the Foxp3 locus and represses Th1- and Th17-associated genes. The preserved viability but reduced Foxp3 expression observed in *Drd2*-deficient Treg cells suggests that Drd2 acts primarily on lineage-maintenance pathways rather than on general survival signals.

These findings also have potential pharmacological implications. Enhancing Drd2 signalling could stabilise Treg cells and strengthen immunoregulatory responses in inflammatory and neurodegenerative conditions. However, systemic Drd2 stimulation would affect neuronal, endocrine and peripheral cell populations and may produce effects unrelated or even opposed to those mediated by Treg cells. Furthermore, the ability of Drd2 to form heteromers with Drd3 introduces an additional level of pharmacological complexity. Strategies directed specifically towards immune-cell Drd2, peripherally restricted ligands, or *ex vivo* modulation of Treg cells before adoptive transfer may therefore offer greater selectivity.

In conclusion, our findings identify Drd2 as an important regulator of Treg differentiation, phenotypic stability and suppressive function. Drd2 signalling in CD4$^+$ T-cells limits dopaminergic neurodegeneration and motor impairment in an αSyn-driven model of Parkinson's disease, while Drd2 expressed by Treg cells is required for effective control of intestinal inflammation. These results establish a previously underappreciated connection between dopaminergic immunoregulation, Treg stability and the gut–brain axis, and support Drd2 as a potential target for strategies aimed at restoring immune tolerance in Parkinson's disease and other inflammation-associated disorders.

Materials and Methods

Study approval

All procedures and housing of mice were compliant with the recommendations in the 8th edition of the Guide for the Care and Use of Laboratory Animals and with the United States Public Health Service Policy. The protocol was approved by the IACUC of Fundación Ciencia & Vida (Permit Number: P016-2020).

Animals

Wild-type C57BL/6J (*CD45.2*$^{+/+}$; JAX Stock No. 000664), congenic B6.SJL-Ptprc^{a} Pepc^{b}/BoyJ (*CD45.1*$^{+/+}$; JAX Stock No. 002014), *CD4*^{Cre} [B6.Cg-Tg(Cd4-cre)1Cwi/BfluJ; JAX Stock No. 017336], *CD8*^{Cre} [C57BL/6-Tg(Cd8a-cre)B8Asin/J; JAX Stock No. 008766], and *Foxp3*^{GFP} reporter mice [B6.Cg-Foxp3^{tm2Ayr}/J] were obtained from The Jackson Laboratory (Bar Harbor, ME, USA). *Drd2*$^{flox/flox}$ (*Drd2*$^{f/f}$) mice were kindly provided by Dr. Jiawei Zhou (Shao et al., 2013).

CD4 ^{Cre} *Drd2* $^{f/f}$, *CD8*^{Cre}*Drd2*$^{f/f}$, *CD4*^{Cre}*Drd2*$^{f/f}$*Foxp3*^{GFP}, and *CD45.1*$^{+/-}$*CD45.2*$^{+/-}$ mice were generated by intercrossing the corresponding parental mouse strains. We confirmed the genotype of these new strains by PCR of genomic DNA and by flow cytometry of peripheral blood cells (for GFP). Male mice were used in all experiments. All mice were housed in plastic homecages in a temperature-controlled room, under a 12:12 h light cycle. The environment was enriched with sterile cardboard cones. All animals had *ad libitum* access to a commercial rodent diet (LABDIET® JL Rat & Mouse/Auto 6F) and filtered, decalcified drinking water.

Experimental mice were monitored daily using a clinical scoring system ranging from 0 to 12, based on four parameters: body weight loss (0–3), general clinical condition (0–3), spontaneous behaviour (0–3), and stool consistency (0–3). Mice reaching a cumulative score of ≥ 7 were humanely euthanised by CO_2 overdose. Animals with a score < 7 that exhibited difficulty eating or drinking received supportive care, including hydrated food in the form of wet gel diet. All animal procedures were approved by the Institutional Animal Care and Use Committee (IACUC) of Fundación Ciencia & Vida and were conducted in accordance with institutional guidelines.

Viral vectors

Adenovirus associated vectors (AAV2) encoding for *SNCA* [NM_001375288.1]:IRES: mRFP1 under the control of the CMV early enhancer fused to modified chicken beta actin (CAG) promoter were obtained from VectorBuilder. The final vector concentration was 10^{13} vg/mL.

Stereotaxic delivery of AAV-αSyn in the SN

The surgical procedures were performed as previously described (Elgueta et al., 2022). Briefly, mice received pre-emptive analgesia with carprofen (5 mg/kg, s.c.) prior to surgery and were anaesthetised with isoflurane (5% for induction and 1.5–2% for maintenance). Once a surgical plane of anaesthesia was achieved, the animals were placed in a stereotaxic frame (Stoelting, Wood Dale, IL, USA), and 1 µL of AAV2-CAG-*SNCA*:IRES:mRFP1 (AAV-αSyn) was injected into the right substantia nigra using the following stereotaxic coordinates: anteroposterior − 2.8 mm from bregma, mediolateral + 1.4 mm from the midline, and dorsoventral − 7.2 mm from the dural surface (Paxinos and Franklin, 2001). Injections were performed at a rate of 0.2 µL every 30 s using a 10-µL Hamilton syringe fitted with a glass capillary. The needle was left in place for 5 min after injection before being slowly withdrawn. The incision was closed with Silkam® sutures (B. Braun), and postoperative analgesia with carprofen (5 mg/kg, s.c.) was administered every 12 h for 3 days.

Beam test

We used a simplified version of the beam test previously described (Fleming et al., 2004). Briefly, the beam apparatus was made of plexiglas and consisted of one horizontal tract of 25 cm length and 2 cm width. The beam surface was covered by a metallic grid (1 cm^2). Mice were videotaped while traversing the grid-surface beam from one of the extremes of the beam to the opposite extreme, where the home-cage was located. Two days of training were performed for habituation to the task. The number of errors (# errors) was quantified by watching the videos in slow-motion mode. An error was defined as when a forelimb or hindlimb slipped through the grid and became visible between the grid and the beam surface or on the side of the grid during a forward movement.

Brain tissue processing

Mice were deeply anaesthetised with 5% isoflurane (Baxter), euthanised under deep anaesthesia, and transcardially perfused with phosphate-buffered saline (PBS). For histological techniques, brains were removed, fixed with 4% paraformaldehyde (Merck, Darmstadt, Germany) in 0.125 M phosphate buffered saline (PBS, pH 7.4), and then cryoprotected for 48 h in 20% glycerine and 2% DMSO in PBS.

Immunohistochemical and immunofluorescent analysis

To carry out immunohistochemical and immunofluorescent analysis, free floating sections (40 µm thick) were processed at the same time in each experiment. For immunohistochemical analysis, sections were washed with PBS and endogenous peroxidase activity was inactivated by 30 min incubation with 0.03% H_2O_2 in methanol (Sigma-Aldrich). After washing three times with PBS, the tissue was incubated for 40 min with blocking solution [4% goat serum, 0.05% Triton X-100 (Sigma-Aldrich) and 4% BSA (Merck, Darmstadt, Germany) in PBS] and exposed overnight to the primary antibodies diluted in blocking solution at room temperature. The primary antibody used was rabbit anti-tyrosine hydroxylase (TH) pAb (1:1000; Millipore, Temecula, CA, USA). For colorimetric immunohistochemistry, antibody binding was

detected by incubating sections with biotinylated goat anti-rabbit secondary pAb (1:500; Jackson ImmunoResearch Laboratories, West Gore, PA, USA) in blocking solution for 2 h at room temperature. The biotinylated antibody was detected by incubation with peroxidase-conjugated avidin (1:5000; Sigma-Aldrich) for 90 min at room temperature followed by incubation with 0.05% diaminobenzidine (Sigma-Aldrich) in 0.03% H_2O_2/Trizma-HCl buffer (pH 7.6). Sections were mounted on glass slides in a 0.2% solution of gelatine in 0.05 M Tris (pH 7.6) (Sigma-Aldrich). The mean number of TH^+ neurons from six SN *pars compacta* (SNpc) sections (separated by 120 µm in between each other) per mouse was blinded quantified under light microscopy at a magnification of 200X, and the total area of SNpc was calculated using ImageJ software (National Institutes of Health, Bethesda, MD). Density of dopaminergic neurons was expressed as the number of TH^+ neurons per area (mm^2) in the SNpc.

For immunofluorescence analysis, brain slices were washed three times with PBS containing 0.02% tween20 and then antigenic recovery was performed with buffer citrate [100 mM citric acid, 100 mM sodium citrate; pH6] at 90°C for 30 min, and then moved on a glass slide and kept at room temperature for 15 min. Brain slices were washed three times with PBS containing 0.02% tween20, and then incubated with blocking solution [0.01% tween20 (both from Sigma-Aldrich) and 3% BSA (Merck, Darmstadt, Germany) in PBS] at room temperature for 1 h, and exposed overnight to the primary antibodies (Rabbit anti-TH diluted 1:250, obtained from Millipore cat# AB152; Rabbit anti-Iba1 diluted 1:1000, obtained from Wako cat# 019-19741; Sheep anti-TREM2 diluted 1:100, obtained from ThermoFisher cat# PA5-46978; rat anti-CD4 diluted 1:250, obtained from Biolegend cat# 100505; and rat anti-CD8 diluted 1:250, obtained from Biolegend cat# 14-0195-82) diluted in blocking solution at 4°C in constant agitation. Brain slices were washed three times with PBS containing 0.02% tween20 and then incubated with the corresponding secondary antibodies: Goat AlexaFluor488-coupled anti-Rabbit (Thermo Fisher Scientific cat# A11008), Donkey AlexaFluor350-coupled anti-Sheep (Thermo Fisher Scientific cat# A21097), Goat AlexaFluor647-coupled anti-Rabbit (Abcam cat# AB150079), Donkey AlexaFluor405-coupled anti-Rat (Thermo Fisher Scientific cat# A48268), Goat AlexaFluor488-coupled anti-Rat (Thermo Fisher Scientific cat# A11006) diluted 1:500 in blocking solution at room temperature and with constant agitation for 2 h. Brain slices were washed three times with PBS containing 0.02% tween20 and, when indicated in figure legends, incubated with DAPI (diluted 1:100.000) at room temperature for 5 min. Brain slices were washed three times with PBS and covered in fuoromount-G. Images were acquired with a fluorescence microscope Leica, Thunder.

Flow cytometry analysis

Cells were stained with Zombie Aqua (ZAq) Fixable Viability kit, followed by fluorochrome-conjugated mAbs specific to cell-surface markers in PBS containing 5% FBS for 15 min. Surface markers analysed included CD4, CD25, CD45, CD45.1, CD45.2, CD44, CD62L, and TCRβ. Afterwards, cells were fixed with 1% paraformaldehyde in phosphate-buffered saline (PBS, Na_2HPO_4 8.1 µM, KH_2PO_4 1.47 µM, NaCl 64.2 mM, KCl 2.68 mM, pH 7.4) for 15 min at room temperature, washed twice with PBS, and analysed in a flow cytometer. For intracellular cytokine staining, $CD4^+$ T-cells were stimulated for 4 h with phorbol-12-myristate-13-acetate (PMA, 50 ng/mL) and ionomycin (1 µg/mL) in the presence of brefeldin A (5 µg/mL,

Life Technologies). Cells were stained with ZAq Fixable Viability kit, followed by cell-surface markers immunostaining in PBS containing 2% FBS. Afterwards, cells were resuspended in fixation/permeabilization solution and incubated for, at least, 30 min. Then, intracellular immunostaining with antibodies to IL-10, IL-17, IFNγ, TGFβ, and TNFα was carried out in permeabilization buffer at 4ºC for 1 h. Data were collected with a Canto II (BD) and results were analysed with FACSDiva (BD) and FlowJo software (Tree Star, Ashlan, OR, USA). All analyses were controlled in a first step with the autofluorescence and in a second step with Fluorescence Minus One (FMO).

In vitro generation of inducible Treg (iTreg)

To induce the differentiation to iTreg, freshly purified naive $CD4^+$ $CD62L^+$ $CD44^-$ T-cells were activated with 50 ng/well of plate-bound anti-CD3 mAb and 2 µg/mL soluble anti-CD28 mAb on flat-bottom 96-well plates (Thermo Scientific), in the presence of 5 ng/mL TGF-β1, 10 ng/mL IL-2, 1µg/mL anti-IFNγ mAb and 100 nM RA. After incubation for 5 d, GFP (Foxp3) expression was analysed to determine the extent of phenotypic Treg differentiation.

DSS-induced colitis

Experimental groups were made by selecting male mice randomly and paired by age. Mice displaying dwarfism or malformations were excluded a *priori*. Mouse groups with different treatments and/or genotypes were kept in different cages to avoid confounding factors. For blinding evaluation, JC or VU was the investigator who knew the identity of the evaluated mice. Mice were treated with 2% DSS in the drinking water. DSS was given for a total period of three days and then replaced with normal drinking water and kept for seven additional days. Body weight was daily recorded throughout the time-course of disease development. The extent of loss of the initial body weight was used as the main parameter to determine disease severity. At the end of the experiment, mice were euthanised under deep anaesthesia to obtain the cLP. Outcome measure: the percentage of body weight loss respective to the initial body weight.

In vivo determination of Treg migration and phenotypic stability

Splenic Treg cells ($CD4^+GFP^+$) isolated from *Foxp3^{GFP} Drd2$^{f/f}$ CD45.1$^{+/+}$* or *Foxp3^{GFP} CD4^{Cre} Drd2$^{f/f}$ CD45.2$^{+/+}$* mice were i.p. injected ($7x10^5$ cells per mouse) into *CD45.1$^{+/-}$ CD45.2$^{+/-}$* recipient mice pre-treated with DSS 2% for three days. Mice were kept with normal drinking water for seven additional days and then sacrificed, and the relative composition ($CD45.1^+$ versus $CD45.2^+$) on $CD4^+$ T-cells and the frequency of GFP expression on donor cells (harbouring single expression of $CD45.1^+$ or $CD45.2^+$) were determined in the cLP. Outcome measure: Quantification of the relative abundance of $CD45.1^+$ or $CD45.2^+$ $CD4^+$ T-cells was conducted to calculate donor Treg recruitment into the cLP. Frequency of GFP^+ cells from donor $CD45.1^+$ or $CD45.2^+$ $CD4^+$ T-cells was conducted to calculate Treg phenotypic stability.

Statistical analysis

Normality of data was assessed using the Shapiro-Wilk test. For data with normal distribution, significant differences were calculated with a two-tailed unpaired Student's *t*-test when comparing only two groups and with one-way ANOVA when comparing more than two groups with only one variable (treatment or genotype). Two-way ANOVA was used to analyse differences in experiments comparing distinct genotypes and/or treatments. For data displaying non-normal distribution, Kruskal-Wallis test was used to compare more than two experimental groups. All analyses were conducted using the GraphPad Prism 11 Software. *p*-values < 0.05 were considered significant.

Declarations

Author Contribution

R.P. designed the study. J.M.J., D.E., O.C., V.U., N.M., and J. Cea conducted experiments using the AAV model and acquired the corresponding data. J. Castro, J.M.J., J.M., and C.P. conducted experiments using the DSS model and performed the in vitro experiments, acquiring the corresponding data. J. Castro, J.M.J., O.C., V.U., N.M., J. Cea, J.M., C.P., and R.P. analysed data from the in vitro and animal experiments and contributed to the interpretation of the results. A.E., S.V., and M.R. generated the mouse strains and established the experimental conditions for the AAV model. C.P., M.R., and J.M.J. critically revised the manuscript. R.P. wrote the manuscript. All authors read and approved the final manuscript.

Acknowledgement

We thank Dr. Jiawei Zhou for kindly providing the Drd2f/f mice. This work was supported by "Financiamiento Basal para Centros Científicos y Tecnológicos de Excelencia de ANID" Centro Ciencia & Vida, FB210008 (to Fundación Ciencia & Vida). This work was also funded by grants FONDECYT-3220328 (to J.M.J.) and FONDECYT-1250021 (to R.P.) from "Agencia Nacional de Investigación y Desarrollo de Chile (ANID)".

DATA AVAILABILITY

All data supporting the findings of this study are available within the paper.

References

1. Alexander SPH et al (2023) The Concise Guide to PHARMACOLOGY 2023/24: G protein-coupled receptors. Br J Pharmacol 180(Suppl 2):S23–S144
2. Besser MJ, Ganor Y, Levite M (2005) Dopamine by itself activates either D2, D3 or D1/D5 dopaminergic receptors in normal human T-cells and triggers the selective secretion of either IL-10, TNFalpha or both. J Neuroimmunol 169:161–171

3. Braak H, Del Tredici K, Rub U, de Vos RA, Jansen Steur EN, Braak E (2003) Staging of brain pathology related to sporadic Parkinson's disease. Neurobiol Aging 24:197–211
4. Campos-Acuna J, Elgueta D, Pacheco R (2019) T-Cell-Driven Inflammation as a Mediator of the Gut-Brain Axis Involved in Parkinson's Disease. Front Immunol 10:239
5. Chen X, Wu X, Zhou Q, Howard OM, Netea MG, Oppenheim JJ (2013) TNFR2 is critical for the stabilization of the CD4 + Foxp3+ regulatory T. cell phenotype in the inflammatory environment. J Immunol 190:1076–1084
6. Contreras F, Prado C, Gonzalez H, Franz D, Osorio-Barrios F, Osorio F, Ugalde V, Lopez E, Elgueta D, Figueroa A, Lladser A, Pacheco R (2016) Dopamine Receptor D3 Signaling on CD4 + T Cells Favors Th1- and Th17-Mediated Immunity. J Immunol 196:4143–4149
7. Deczkowska A, Keren-Shaul H, Weiner A, Colonna M, Schwartz M, Amit I (2018) Disease-Associated Microglia: A Universal Immune Sensor of Neurodegeneration. Cell 173:1073–1081
8. Elgueta D, Chovar O, Ugalde V, Sanchez-Guajardo V, Catenaccio A, Court F, Pacheco R (2022) Analyzing the Parkinson's Disease Mouse Model Induced by Adeno-associated Viral Vectors Encoding Human alpha-Synuclein. J Vis Exp
9. Elgueta D, Aymerich MS, Contreras F, Montoya A, Celorrio M, Rojo-Bustamante E, Riquelme E, Gonzalez H, Vasquez M, Franco R, Pacheco R (2017) Pharmacologic antagonism of dopamine receptor D3 attenuates neurodegeneration and motor impairment in a mouse model of Parkinson's disease. Neuropharmacology 113:110–123
10. Elgueta D, Contreras F, Prado C, Montoya A, Ugalde V, Chovar O, Villagra R, Henriquez C, Abellanas MA, Aymerich MS, Franco R, Pacheco R (2019) Dopamine Receptor D3 Expression Is Altered in CD4 + T-Cells From Parkinson's Disease Patients and Its Pharmacologic Inhibition Attenuates the Motor Impairment in a Mouse Model. Frontiers in immunology 10
11. Fleming SM, Salcedo J, Fernagut PO, Rockenstein E, Masliah E, Levine MS, Chesselet MF (2004) Early and progressive sensorimotor anomalies in mice overexpressing wild-type human alpha-synuclein. J Neurosci 24:9434–9440
12. Franz D, Contreras F, Gonzalez H, Prado C, Elgueta D, Figueroa C, Pacheco R (2015) Dopamine receptors D3 and D5 regulate CD4(+)T-cell activation and differentiation by modulating ERK activation and cAMP production. J Neuroimmunol 284:18–29
13. Galiano-Landeira J, Torra A, Vila M, Bove J (2020) CD8 T cell nigral infiltration precedes synucleinopathy in early stages of Parkinson's disease. Brain 143:3717–3733
14. Garg G et al (2019) Blimp1 Prevents Methylation of Foxp3 and Loss of Regulatory T Cell Identity at Sites of Inflammation. Cell Rep 26:1854–1868e1855
15. Gonzalez H, Pacheco R (2014) T-cell-mediated regulation of neuroinflammation involved in neurodegenerative diseases. J Neuroinflamm 11:201
16. Gonzalez H, Contreras F, Pacheco R (2015) Regulation of the Neurodegenerative Process Associated to Parkinson's Disease by CD4 + T-cells. J neuroimmune pharmacology: official J Soc NeuroImmune Pharmacol 10:561–575

17. Gonzalez H, Contreras F, Prado C, Elgueta D, Franz D, Bernales S, Pacheco R (2013) Dopamine Receptor D3 Expressed on CD4 + T Cells Favors Neurodegeneration of Dopaminergic Neurons during Parkinson's Disease. J Immunol 190:5048–5056
18. Helmin KA, Morales-Nebreda L, Torres Acosta MA, Anekalla KR, Chen SY, Abdala-Valencia H, Politanska Y, Cheresh P, Akbarpour M, Steinert EM, Weinberg SE, Singer BD (2020) Maintenance DNA methylation is essential for regulatory T cell development and stability of suppressive function. J Clin Invest 130:6571–6587
19. Huber S, Schramm C, Lehr HA, Mann A, Schmitt S, Becker C, Protschka M, Galle PR, Neurath MF, Blessing M (2004) Cutting edge: TGF-beta signaling is required for the in vivo expansion and immunosuppressive capacity of regulatory CD4 + CD25+ T cells. J Immunol 173:6526–6531
20. Kim C, Ho DH, Suk JE, You S, Michael S, Kang J, Joong Lee S, Masliah E, Hwang D, Lee HJ, Lee SJ (2013) Neuron-released oligomeric alpha-synuclein is an endogenous agonist of TLR2 for paracrine activation of microglia. Nat Commun 4:1562
21. Lee PP, Fitzpatrick DR, Beard C, Jessup HK, Lehar S, Makar KW, Perez-Melgosa M, Sweetser MT, Schlissel MS, Nguyen S, Cherry SR, Tsai JH, Tucker SM, Weaver WM, Kelso A, Jaenisch R, Wilson CB (2001) A critical role for Dnmt1 and DNA methylation in T cell development, function, and survival. Immunity 15:763–774
22. Lim KL, Zhang CW (2013) Molecular events underlying Parkinson's disease - an interwoven tapestry. Front Neurol 4:33
23. Lindestam Arlehamn CS, Dhanwani R, Pham J, Kuan R, Frazier A, Rezende Dutra J, Phillips E, Mallal S, Roederer M, Marder KS, Amara AW, Standaert DG, Goldman JG, Litvan I, Peters B, Sulzer D, Sette A (2020) alpha-Synuclein-specific T cell reactivity is associated with preclinical and early Parkinson's disease. Nat Commun 11:1875
24. Liu Z, Zhai XR, Du ZS, Xu FF, Huang Y, Wang XQ, Qiu YH, Peng YP (2021) Dopamine receptor D2 on CD4(+) T cells is protective against neuroinflammation and neurodegeneration in a mouse model of Parkinson's disease. Brain Behav Immun 98:110–121
25. Lu JH, Liu YQ, Deng QW, Peng YP, Qiu YH (2015) Dopamine D2 Receptor Is Involved in Alleviation of Type II Collagen-Induced Arthritis in Mice. Biomed Res Int 2015:496759
26. Maekawa Y, Minato Y, Ishifune C, Kurihara T, Kitamura A, Kojima H, Yagita H, Sakata-Yanagimoto M, Saito T, Taniuchi I, Chiba S, Sone S, Yasutomo K (2008) Notch2 integrates signaling by the transcription factors RBP-J and CREB1 to promote T cell cytotoxicity. Nat Immunol 9:1140–1147
27. Mora J, Raich I, Ugalde V, Navarro G, Prado C, Vidal PM, Leal P, Espinoza A, Liu M, Weersma R, Gacesa R, Hermoso MA, Franco R, Pacheco R (2025) The Heteromeric Dopamine Receptor D2:D3 Controls the Gut Recruitment and Suppressive Activity of Regulatory T-Cells. Int J Mol Sci 26
28. Noelker C, Morel L, Lescot T, Osterloh A, Alvarez-Fischer D, Breloer M, Henze C, Depboylu C, Skrzydelski D, Michel PP, Dodel RC, Lu L, Hirsch EC, Hunot S, Hartmann A (2013) Toll like receptor 4 mediates cell death in a mouse MPTP model of Parkinson disease. Sci Rep 3:1393

29. Pacheco R (2021) T-cell based immunotherapies for Parkinson’s disease. Explor Neuroprotective Therapy 1:72–85
30. Pacheco R, Contreras F, Zouali M (2014) The dopaminergic system in autoimmune diseases. Front Immunol 5:117
31. Reynolds AD, Banerjee R, Liu J, Gendelman HE, Mosley RL (2007) Neuroprotective activities of CD4 + CD25+ regulatory T cells in an animal model of Parkinson's disease. J Leukoc Biol 82:1083–1094
32. Roodveldt C, Bernardino L, Oztop-Cakmak O, Dragic M, Fladmark KE, Ertan S, Busra A, Pita C, Ciglar L, Garraux G, Williams-Gray C, Pacheco R, Romero-Ramos M (2024) The immune system in Parkinson's disease: what we know so far. a journal of neurology, Brain
33. Rubtsov YP, Rasmussen JP, Chi EY, Fontenot J, Castelli L, Ye X, Treuting P, Siewe L, Roers A, Henderson WR Jr., Muller W, Rudensky AY (2008) Regulatory T cell-derived interleukin-10 limits inflammation at environmental interfaces. Immunity 28:546–558
34. Shao W, Zhang SZ, Tang M, Zhang XH, Zhou Z, Yin YQ, Zhou QB, Huang YY, Liu YJ, Wawrousek E, Chen T, Li SB, Xu M, Zhou JN, Hu G, Zhou JW (2013) Suppression of neuroinflammation by astrocytic dopamine D2 receptors via alphaB-crystallin. Nature 494:90–94
35. Sokoloff P, Giros B, Martres MP, Bouthenet ML, Schwartz JC (1990) Molecular cloning and characterization of a novel dopamine receptor (D3) as a target for neuroleptics. Nature 347:146–151
36. Sulzer D et al (2017) T cells from patients with Parkinson's disease recognize alpha-synuclein peptides. Nature 546:656–661
37. Ugalde V, Contreras F, Prado C, Chovar O, Espinoza A, Pacheco R (2021) Dopaminergic signalling limits suppressive activity and gut homing of regulatory T cells upon intestinal inflammation. Mucosal Immunol 14:652–666
38. Wu W, Sun M, Zhang HP, Chen T, Wu R, Liu C, Yang G, Geng XR, Feng BS, Liu Z, Liu Z, Yang PC (2014) Prolactin mediates psychological stress-induced dysfunction of regulatory T cells to facilitate intestinal inflammation. Gut 63:1883–1892
39. Zhu J, Hu Z, Han X, Wang D, Jiang Q, Ding J, Xiao M, Wang C, Lu M, Hu G (2018) Dopamine D2 receptor restricts astrocytic NLRP3 inflammasome activation via enhancing the interaction of beta-arrestin2 and NLRP3. Cell Death Differ 25:2037–2049

Figures

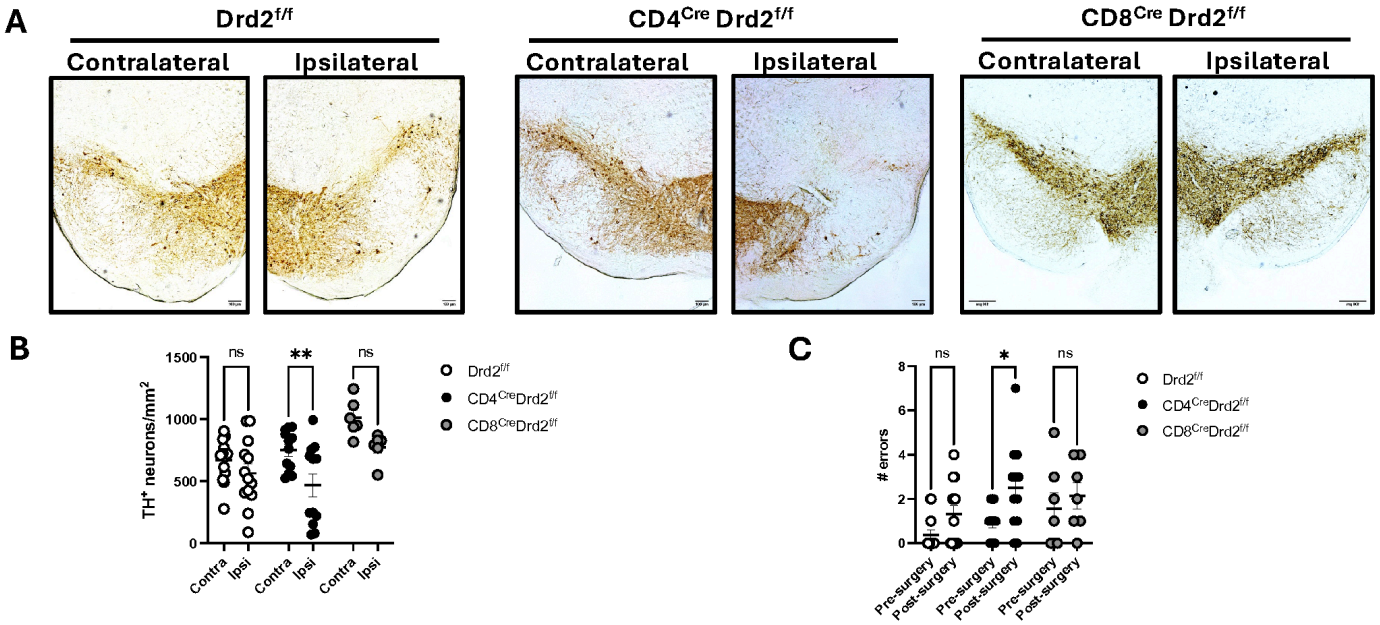


Figure 1. The selective deficiency of *Drd2* in CD4⁺ T-cells increases neurodegeneration of dopaminergic neurons and motor decline in AAV-αSyn-treated mice. *Drd2*$^{f/f}$ (white symbols), *CD4*^{Cre}*Drd2*$^{f/f}$ (black symbols), and *CD8*^{Cre}*Drd2*$^{f/f}$ (grey symbols) mice received unilateral stereotaxic injections of AAV-hαSyn (10^{10} vg/mice) in the right SN (ipsilateral). Sixteen weeks later, the motor performance was determined followed by the quantification of the extent of dopaminergic neuron loss by immunohistochemical (IHC) analysis of TH in the SN. (**A**) Representative images obtained for IHC analyses of TH are shown. Left SN were analysed as internal controls (contralateral). Scale bars, 100 µm. (**B**) Quantification of TH+ neurons per area in the SNpc. (**C**) The number of errors was quantified using the beam test. (B,C) Each symbol represents an individual mouse; n = 7-13 mice per group. Mean ± SEM are shown. *, p<0.05; **, p<0.01 by two-ways ANOVA followed by the Sidak's multiple comparison test. ns, non-significant.

Figure 1

See image above for figure legend.

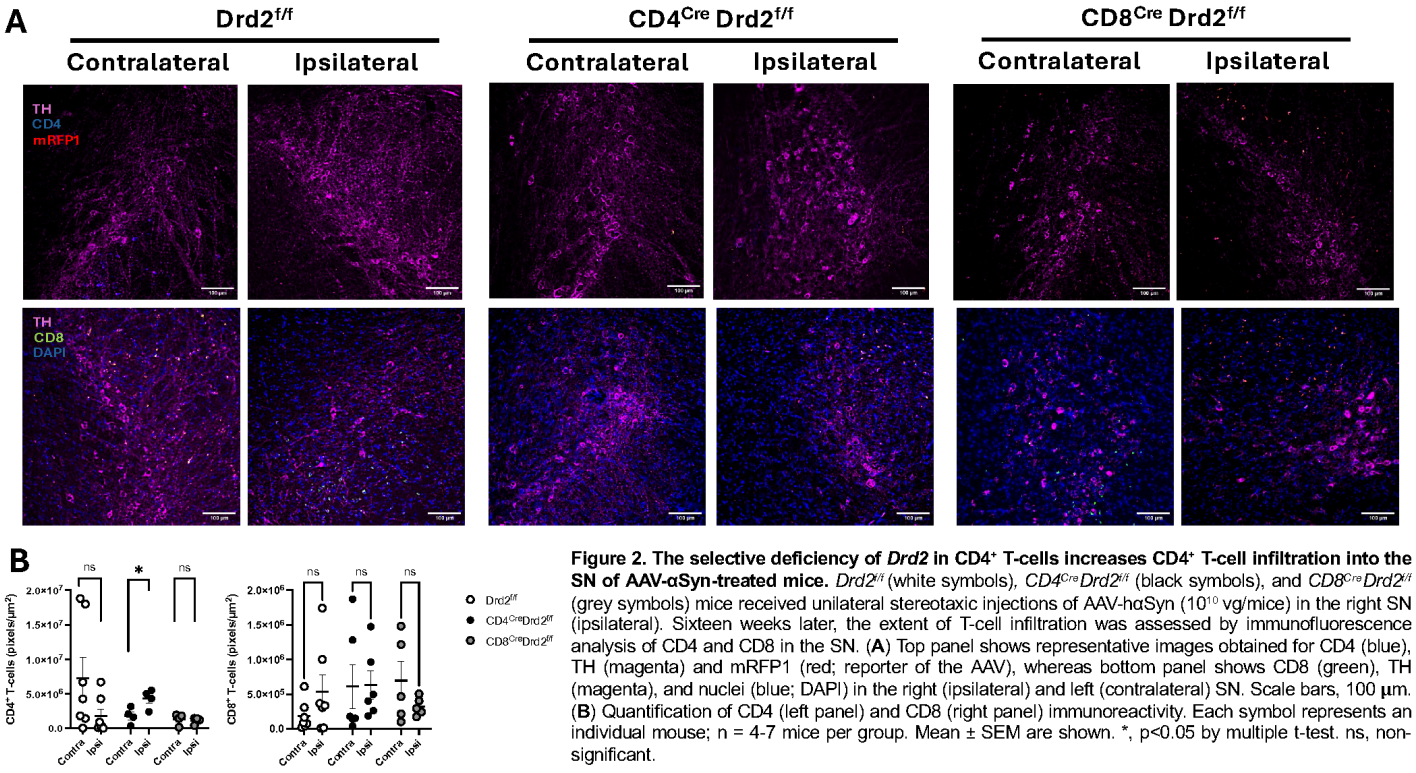


Figure 2. The selective deficiency of *Drd2* in CD4⁺ T-cells increases CD4⁺ T-cell infiltration into the SN of AAV-αSyn-treated mice. *Drd2*$^{f/f}$ (white symbols), *CD4*^{Cre}*Drd2*$^{f/f}$ (black symbols), and *CD8*^{Cre}*Drd2*$^{f/f}$ (grey symbols) mice received unilateral stereotaxic injections of AAV-hαSyn (10^{10} vg/mice) in the right SN (ipsilateral). Sixteen weeks later, the extent of T-cell infiltration was assessed by immunofluorescence analysis of CD4 and CD8 in the SN. (**A**) Top panel shows representative images obtained for CD4 (blue), TH (magenta) and mRFP1 (red; reporter of the AAV), whereas bottom panel shows CD8 (green), TH (magenta), and nuclei (blue; DAPI) in the right (ipsilateral) and left (contralateral) SN. Scale bars, 100 µm. (**B**) Quantification of CD4 (left panel) and CD8 (right panel) immunoreactivity. Each symbol represents an individual mouse; n = 4-7 mice per group. Mean ± SEM are shown. *, p<0.05 by multiple t-test. ns, non-significant.

Figure 2

See image above for figure legend.

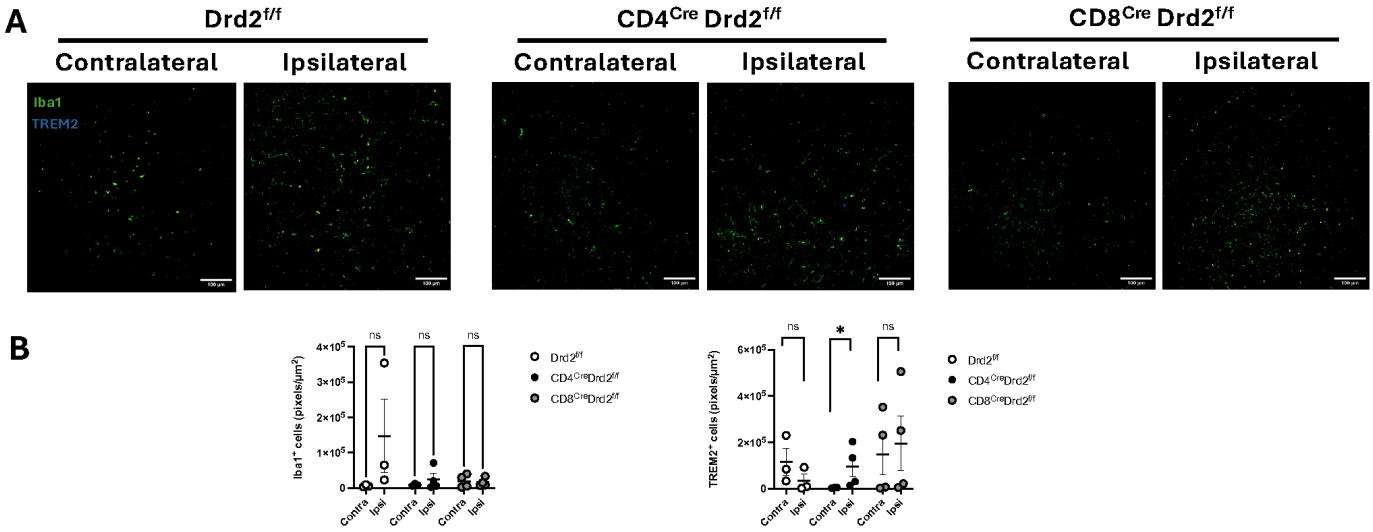


Figure 3. The selective deficiency of *Drd2* in CD4⁺ T-cells increases TREM2-associated microglia in the SN of AAV-αSyn-treated mice. *Drd2*$^{f/f}$ (white symbols), *CD4*^{Cre}*Drd2*$^{f/f}$ (black symbols), and *CD8*^{Cre}*Drd2*$^{f/f}$ (grey symbols) mice received unilateral stereotaxic injections of AAV-hαSyn (10^{10} vg/mice) in the right SN (ipsilateral). Sixteen weeks later, the extent of reactive microglia was assessed by immunofluorescence analysis of Iba1 and TREM2 in the SN. (**A**) Representative images obtained for Iba1 (green) and TREM2 (blue) in the right (ipsilateral) SN are shown. Left SN were analysed as internal controls (contralateral). Scale bars, 100 µm. (**B**) Quantification of Iba1 (left panel) and TREM2 (right panel) immunoreactivity. Each symbol represents an individual mouse; n = 3-4 mice per group. Mean ± SEM are shown. *, p<0.05 by multiple t-test. ns, non-significant.

Figure 3

See image above for figure legend.

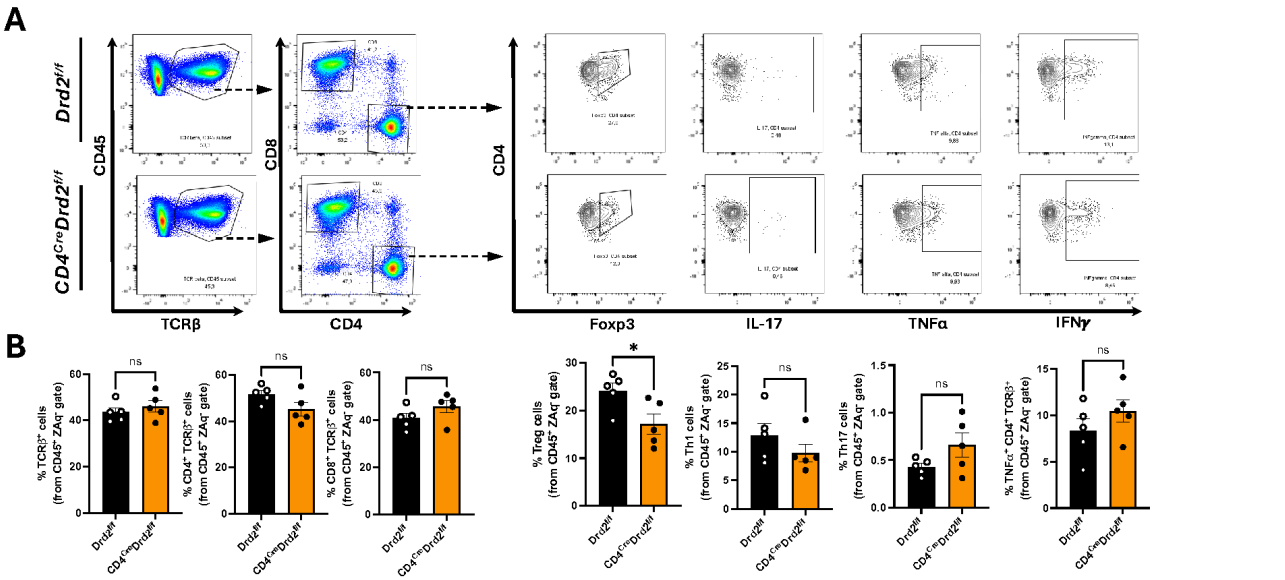


Figure 4. *Drd2* deficiency in T-cells is associated with a reduction on the frequency of Tregs in the spleen of AAV-αSyn-treated mice. *Drd2*$^{f/f}$ (black bars), and *CD4*^{Cre}*Drd2*$^{f/f}$ (orange bars) mice received unilateral stereotaxic injections of AAV-hαSyn (10^{10} vg/mice) in the right SN (ipsilateral). Sixteen weeks later, the frequency of T-cell subsets was quantified in the spleen by flow cytometry. (**A**) Representative density plots showing the gating strategy for the analysis of TCR**β**$^{+}$ T-cells, CD4^{+} and CD8^{+}, and Treg, Th17, Th1 and TNF**α**-producing functional subsets of CD4^{+} T-cells. Dotted lines indicate the relationship with parental gates. (**B**) Quantification of each particular subset indicated in (A). Each symbol represents an individual mouse; n = 5 mice per group. Mean ± SEM are shown. *, p<0.05 by two-tailed unpaired Student's t-test. ns, non-significant.

Figure 4

See image above for figure legend.

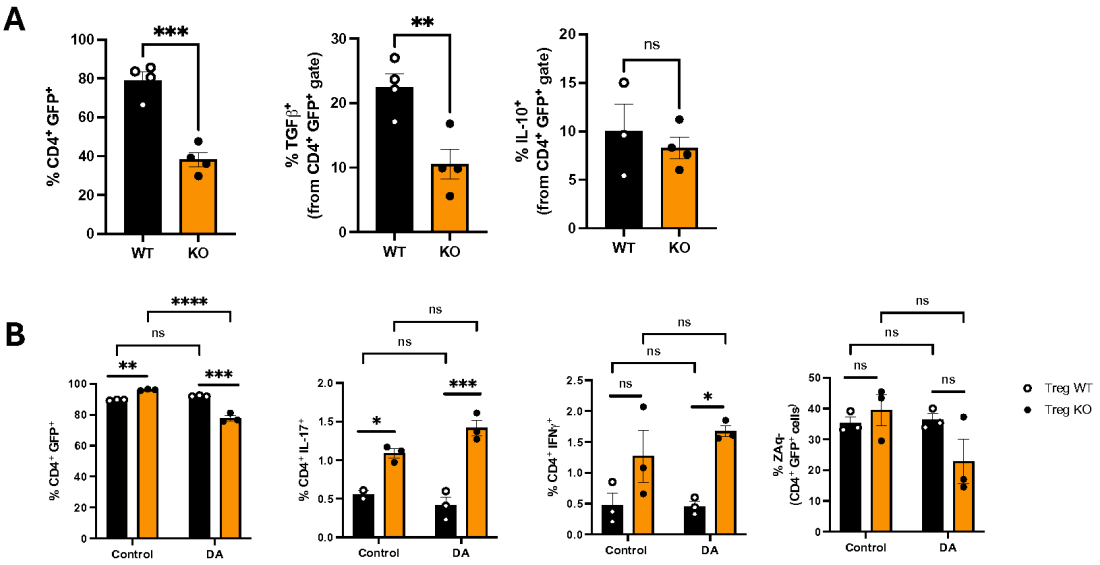


Figure 5. *Drd2* deficiency in T cells results in impaired iTreg generation and reduced phenotypic stability. (**A**) CD4⁺CD25⁺ naive T-cells were isolated from the spleen of *Foxp3*^{GFP} (WT; black bars), and *Foxp3*^{GFP}*CD4*^{Cre}*Drd2*$^{f/f}$ (KO; orange bars) mice and then differentiated into iTreg for 5 d. Left panel shows the percentage of Foxp3 (GFP) expression after iTreg-differentiation. The extent of TGF**β** (middle panel) and IL-10 (right panel) was determined by intracellular immunostaining and analysed by flow cytometry. (**B**) iTreg were stimulated with anti-CD3/CD28 in the presence or absence of dopamine 2 **μ**M (DA) for 72 h and the extent of Foxp3 (GFP) expression, IL-17 and IFN**γ** production and viability (ZAq⁻ cells) were analysed by flow cytometry. (A-B) Each symbol represents data obtained from an individual mouse. Mean ± SEM are shown. *p<0.05; **, p<0.01; ***, p<0.001; ****, p<0.0001 by (A) two-tailed unpaired Student's t-test or (B) two-way ANOVA followed by Sidak's multiple comparison test. ns, non-significant.

Figure 5

See image above for figure legend.

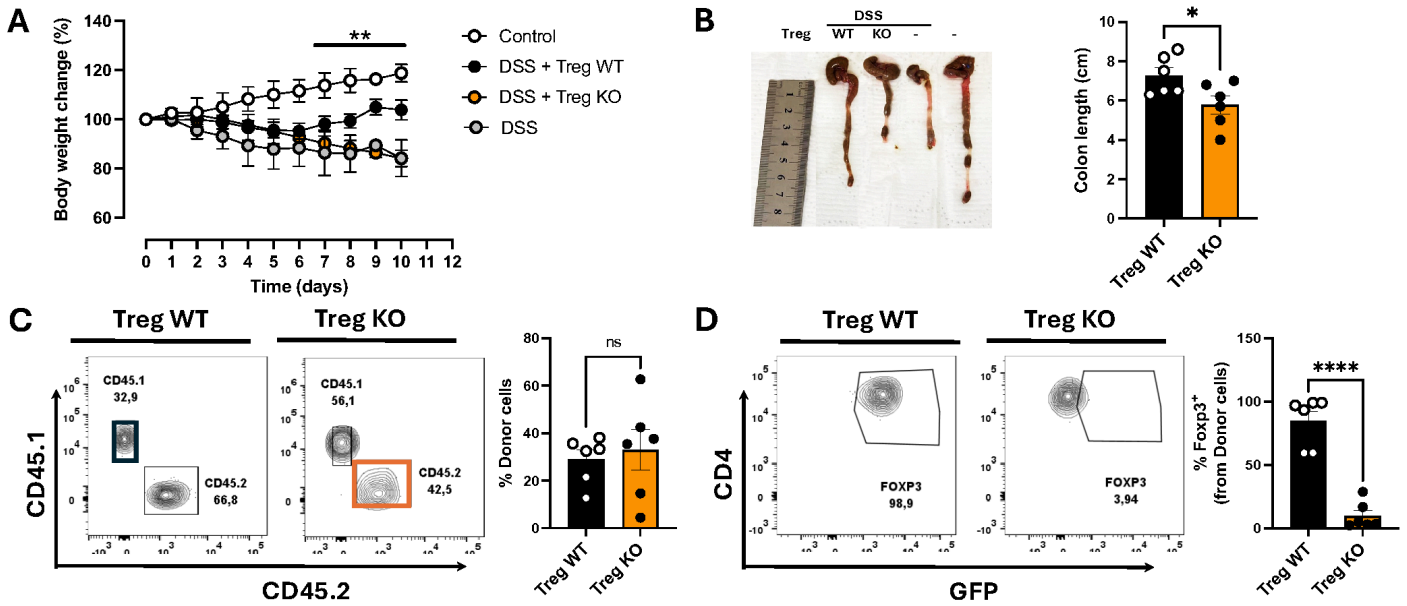


Figure 6. *Drd2* deficiency in T-cells results in impaired phenotypic Treg stability *in vivo*. WT (*CD45.1*$^{+/-}$ *CD45.2*$^{+/-}$) recipient mice received 2% DSS in the drinking water for three days and then maintained for seven additional days with normal water. Splenic Treg cells (CD4$^+$GFP$^+$) were isolated from *Foxp3*^{GFP} *Drd2*$^{f/f}$ *CD45.1*$^{+/+}$ (Treg WT) or *Foxp3*^{GFP} *CD4*^{Cre} *Drd2*$^{f/f}$ *CD45.2*$^{+/+}$ (Treg KO) and i.p. injected (7x10^5 cells per mouse) three days after the beginning of DSS treatment. A group of mice did not receive Treg transfer (group DSS) and another group of mice did not receive neither DSS nor Treg (group control). (**A**) Body weight was daily registered and expressed as percentage of the initial body weight. Statistical differences between DSS+Treg WT and DSS+Treg KO were identified during the last 4 d. (**B**) Colon length was determined at the end-point. Left panel shows representative images. Right panel shows the quantification. (C, D) At the end-point, mononuclear cells were isolated from the colonic lamina propria (cLP) and (**C**) the percentage of donor T-cells and (**D**) the percentage of GFP$^+$ (Foxp3$^+$) donor cells were determined by flow cytometry. Left panels show representative dot plots and right panels show the quantification. (B-D) Each symbol represents an individual mouse. (A-D) Mean ± SEM are shown from 6 mice per group. *, p<0.05, **, p<0.01; ****, p<0.0001 by (A) two-way ANOVA followed by Tukey's multiple comparison test or by (B-D) two-tailed unpaired Student's t-test. ns, non-significant.

Figure 6

See image above for figure legend.